# Surface-Level Path Loss Modelling for Sensor Networks in Flat and Irregular Terrain

POH KIT CHONG, KAIST
DAEYOUNG KIM, KAIST

Many wireless sensor network applications require sensor nodes to be deployed on the ground or other surfaces. However, there has been little effort to characterise the large- and small-scale path loss for surface-level radio communications. We present a comprehensive measurement of path loss and fading characteristics for surface-level sensor nodes in the 400MHz band in both flat and irregular outdoor terrain in an effort to improve the understanding of surface-level sensor network communications performance, and to increase the accuracy of sensor network modelling and simulation. Based on our measurement results, we characterise the spatial small-scale area fading effects as a Rician distribution with a distance-dependent K-factor. We also propose a new semi-empirical path loss model for outdoor surface-level wireless sensor networks called the Surface-Level Irregular Terrain (SLIT) model. We verify our model by comparing measurement results with predicted values obtained from high-resolution digital elevation model (DEM) data and computer simulation for the 400MHz and 2.4GHz band. Finally, we discuss the impact of the SLIT model and demonstrate through simulation the effects when SLIT is used as the path loss model for existing sensor network protocols.

Categories and Subject Descriptors: I.6.5 [**Simulation and Modelling**]: Model Development - Modelling methodologies; I.6.4 [**Simulation and Modelling**]: Model Validation and Analysis; C.2.1 [**Computer-Communication Networks**]: Network Architecture and Design

General Terms: Performance, Design, Simulation

Additional Key Words and Phrases: Modelling of systems and physical environments, Foundations of sensor networks, Simulation tools and environments, Surface level communications

## 1. INTRODUCTION

Many of the current wireless sensor network applications require sensor nodes to be deployed at ground- or surface-level, with the base of the antenna raised only a few centimetres off the surface or even with PCB antennas at ground-level itself [Yoo et al. 2009]. This scenario is expected to be even more pronounced in the future when nodes will be extremely small [Wong and Arvind 2005] and are expected to have antenna elevations measuring mere milimetres off the ground or other surfaces (eg. floor, contain-

ers). In such conditions, Norton surface waves [Norton 1937] may play an important role in the communication between two RF devices.

Surface waves occur because the ground is not a perfect reflector, and its intensity is affected by the surface's characteristics of conductivity and permittivity along the travelled path. Most of the existing works relating to surface wave propagation modelling are for long-range and relatively low-frequency communications like AM radio or high frequency surface wave radars (HFSWR). This is mainly because the effect of surface waves can be neglected if the antennas of devices participating in the tranmission and reception are elevated more than one wavelength $\lambda$ above the surface [Bullington 1947]. Nevertheless, since most sensor networks communicate in the UHF band between 300MHz to 3GHz, nodes placed on the ground fail to meet the criteria to disregard the effects of surface waves. In such cases, surface waves play a significant effect in the transmission of signals [Bullington 1947].

Besides the effects of surface waves, communication near surface level also occurs with most of the first Fresnel zone [Rappaport 2001] blocked by the surface, causing significant diffraction losses. As such, although two communicating devices may be visually within the line-of-sight (LOS) of each other with no visible obstruction in between, the reality is that a significant path loss over free space occurs and should be considered as quasi-LOS. Diffraction, reflection, and scattering of signals cause multipath effects. These multipath waves combine constructively and destructively to create small-scale fading effects that can cause the signal attenuation to vary significantly within a distance of half a wavelength [Hoffman and Cox 1982]. Since most sensor networks consists of static nodes, and small-scale fading is a spatial phenomenon, sensor nodes experience static multipath fading.

Near ground packet transmission and reception measurements for sensor nodes have been carried out in the past [Deepak et al. 2002; Cerpa et al. 2003; Woo et al. 2003; Cerpa et al. 2005; Zhao and Govindan 2003]. However, all these works focused on the packet reception rates of nodes in different environmental conditions rather than attempting to characterise the propagation channel. [Zhou et al. 2004; 2006] carried out experiments to characterise the radio irregularity of wireless sensor networks. Based on experimental results, they proposed a new Radio Irregularity Model (RIM) to account for the anisotropy, continuous variation, and heterogeneity of radio signals. In comparison, our work attempts to model the path loss using terrain information that leads to radio signal irregularity due to the irregular terrain. A few attempts to partially characterise the propagation channel at antenna heights of less than 1m have been made before. However, they either sample too few data points because their focus was on specific human forms (standing, sitting on the floor, or lying prone) and ignore the large-scale path loss characteristics [Foran et al. 1999; Welch et al. 2000] or they disregard small-scale fading [Sohrabi et al. 1999; Joshi et al. 2005; Martfnez-Sala et al. 2005]. [Woyach et al. 2006] showed that the small-scale fading is a function of spatial location for static sensor nodes and is time invariant, but the measurement was performed in an indoor environment on top of a rotating turntable.

In this paper, we attempt to comprehensively measure and characterise the small-scale fading and large-scale path loss of surface-level sensor nodes in the 400MHz band in an outdoor environment in an effort to improve the understanding of surface-level sensor network communications performance, and to increase the accuracy of sensor network modelling and simulation. We start by measuring the small-scale fading characteristics for two different terrains, flat and irregular, and show that in a local area of $0.72\text{m}^2$, the cumulative signal levels is Rician distributed. The medians of the small-scale area signals are then used for comparison with different large-scale path loss models. We demonstrate that the medians of the small-scale area signals are lognormally distributed around the mean large-scale path loss, which can be accurately

predicted using the surface wave model. We also calculate the standard deviation and path loss exponential of the channel. Finally, we propose a more accurate path loss model for surface-level UHF narrowband communications for outdoor irregular terrain called Surface-Level Irregular Terrain (SLIT) model, and verify it by comparing measurement results with predicted values calculated using terrain profiles obtained from high-resolution digital elevation model (DEM) data and computer simulation.

The main contributions of our work are:

— We show through empirical measurements that the surface wave component is an important factor that needs to be considered for an accurate prediction of large-scale path loss for WSN located at surface-level, and that the distribution of the received signal in a small-scale area is Rician distributed.
— We propose the SLIT model as a more accurate path loss model for outdoor irregular terrain by taking into account the surface wave component, and applying effective antenna heights and diffraction gains based on the terrain profile. The usage of the SLIT model allows for a fast and accurate estimation of the large-scale path loss in irregular terrain, and coupled with terrain information (from DEM and other formats), we can perform accurate computer simulations to verify wireless sensor network protocols.

The rest of the sections of this paper are organised as follows. Section 2 provides an overview of related works. Section 3 describes our measurement set up and environment. Section 4 and 5 presents the measurement results for the flat and irregular terrain, respectively, and also the SLIT model. We then empirically verify our model in Section 6. After what, we discuss the impact of the SLIT model and demonstrate the effects of irregular terrain on existing sensor network protocols in Section 7. Finally, we conclude in Section 8.

## 2. RELATED WORKS

A radio signal generated and propagated from a source in the vicinity of the ground generally has a higher path loss than is expected in free space. The earliest works on the transmission of radio wave over the surface of earth (ground-wave) was contributed by Zenneck [Zenneck 1907] and Sommerfeld [Sommerfeld 1909]. Norton [Norton 1937] later built upon their work to develop an improved form for the Hertz potential for arbitrary heights. The current definition of a ground-wave is a wave that is comprised of a Norton surface wave (referred to as just "surface wave" from here on), and a space wave consisting of a direct wave and a ground-reflected wave [IEEE 1998]. In many previous wireless communication applications, the existence of surface waves could largely be ignored because of the raised antennas, and much of the work on surface wave focused on HF applications that have a large $\lambda$. However, in WSNs, nodes are frequently required to be deployed at surface-level, and we examine the effects of surface waves on WSN modelling and applications. A summary of developments in ground-wave research, including surface waves, is given by [Wait 1998].

One of the earliest RF propagation measurement for low-lying antennas for WSN applications was performed by [Sohrabi et al. 1999] for the 800-1000MHz UHF band. The path loss exponent and shadowing variance for a log-normal path loss model was measured for eleven different sites, with a separation distance of up to 30m between antennas. [Joshi et al. 2005] also performed measurements for LOS and forested paths. However, their measurements had a minimum antenna height of 45cm, and did not measure small-scale fading in a localised area. [Welch et al. 2000; Foran et al. 1999] performed measurement of signal strengths for specific human forms (standing, sitting, and lying on the ground), and ignored the large-scale path loss characteristics. [Martfnez-Sala et al. 2005] proposed a 2-slope log-normal path loss prediction model

based on their measurements over 3 locations, with a lower rate of signal decay for a nodes located nearer to the signal source and a steeper rate of decay after a certain distance. [Su and Alzaghal 2009] measured the radiation pattern of MicaZ motes (2.4GHz channel) and the effects of human interference when standing in-between a transmitter-receiver pair. However, the antennas' exact elevation above ground was not stated. [Andersen et al. 1995] also highlighted the necessity of improving wireless protocol models by customising them for different environments, and showed different models that are used for more accurate modelling in different locations and conditions. In this paper, we differ from these existing works by:

— Performing a raster scan at ground level to measure the effects of small-scale fading in a local area, and to find the median signal level for the particular location for large-scale path loss modelling
— We also characterise small-scale fading in local areas with a suitable distribution
— Proposing a more accurate path loss model by including the effects of the surface wave model and terrain profile

Near ground packet transmission and reception measurements for sensor nodes have been carried out in the past [Deepak et al. 2002; Cerpa et al. 2003; Woo et al. 2003; Cerpa et al. 2005; Zhao and Govindan 2003]. However, all these works focused on the packet reception rates (PRRs) of nodes in different environmental conditions rather than attempting to characterise the propagation channel. Most of them show that packet reception rate is time variable and is not an exact function of distance, but the results are not explained. [Zhou et al. 2004; 2006] carried out experiments to characterise the radio irregularity of wireless sensor networks communications. Based on experimental results, they proposed a new Radio Irregularity Model (RIM) to account for the anisotropy, continuous variation, and heterogeneity of radio signals. In comparison, our work attempts to model the radio signal irregularity based on terrain information and is complementary to these previous works by proposing a new surface-level path loss model for irregular terrain. We do not directly measure the packet reception rate; rather, we examine the terrain conditions that may lead to varying signal strengths that can affect the packet reception rates.

## 3. MEASUREMENT EQUIPMENT, ENVIRONMENT, METHODOLOGY, AND CHANNEL MODELS

### 3.1. Measurement Equipment

For our measurements, we used a sensor node developed by SNR [SNR ] that has been used for a military surveillance and reconnaissance pilot project in Korea as the transmitter (T). The sensor node employs a CC1101 [Texas Instruments 2008a] transceiver as its radio, and was set to transmit continuously with a carrier wave (CW) in the 400MHz band. As the receivers, we used an Agilent spectrum analyser and other sensor nodes to measure the amplitude of the CW. All systems were equipped with the same type of $\lambda/4$ whip antenna, a type of omnidirectional antenna that is popularly used in WSNs.

The spectrum analyser was controlled remotely through the GPIB (General Purpose Interface Bus) interface and traces were captured directly into a laptop. The receiver sensor nodes were configured to measure the RSSI value every 5ms. This setting allows a constant sampling of the channel, and is similar or higher than the sampling rates used in previous work [Hoffman and Cox 1982; Kajiwara 2000; Hashim and Stavrou 2005].

The receiver sensor nodes were calibrated using the spectrum analyser, which has an amplitude accuracy of $\pm 2.03$dB at 0 to 55 °C for the 400MHz frequency band. Fig. 1 shows the measured signal strength at the spectrum analyser and sensor nodes versus
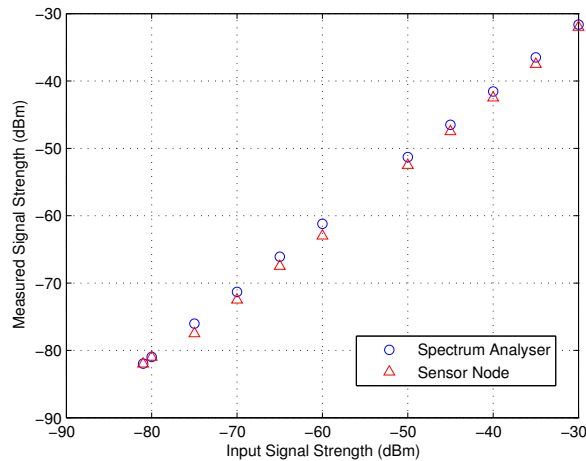
Fig. 1. Scatter plot of measured signal versus input signal

the input signal strength after calibration. As can be seen from the figure, the sensor nodes give a relatively accurate value of the signal strength compared to the spectrum analyser. The range where the RSSI (Received Signal Strength Indicator) readout is linear can be found in [Texas Instruments 2008a]. The reasons for using the sensor nodes as receivers are mainly because of the difficulty in transporting the spectrum analyser in irregular terrain where we would be performing the measurements and the fast RSSI readout response time for the CC1101 transceiver (between 155 and $310\mu$s depending on the filter length [Texas Instruments 2008b].

### 3.2. Measurement Environment

We performed the measurements in three different environments as detailed below:

— Location I - Two football (soccer) fields next to each other measuring 50m x 90m and 60m x 100m, respectively. The fields are flat and sparsely covered with short grass that did not block the visual LOS between nodes.
— Location II - A hilly area with slope gradients between 6 and 25° (Fig. 2). The ground is covered by leafy vegetation in summer and fall, and is also populated by a mix of trees with coniferous and simple, deciduous leaves. However, we report only measurements performed in winter here since our aim is to model the path loss caused by the irregular terrain and to avoid the fading effects from wind-blown foliage [Kajiwara 2000]. The terrain is highly irregular with few LOS paths.
— Location III - A plain which is covered in metre-high reedy grass and some small shrubs interspersed with some 3m tall petiolated, compound leaf trees. Similar to Location II, only measurement performed in winter is used to avoid the effects of wind-blown foliage.

### 3.3. Measurement Methodology

To measure the fading and path loss at a local area, we follow the measurement methodology first mentioned by [Hoffman and Cox 1982] and similar to that performed by [Cox et al. 1983]. The transmitter was first placed at ground-level at a random location with the antenna upright, and then turned on. We then held the receiving antenna, attached to a 1.5m long pole and sampling the channel every 5ms, at about 2-3cm above the surface-level at another position and performed a raster scan over an
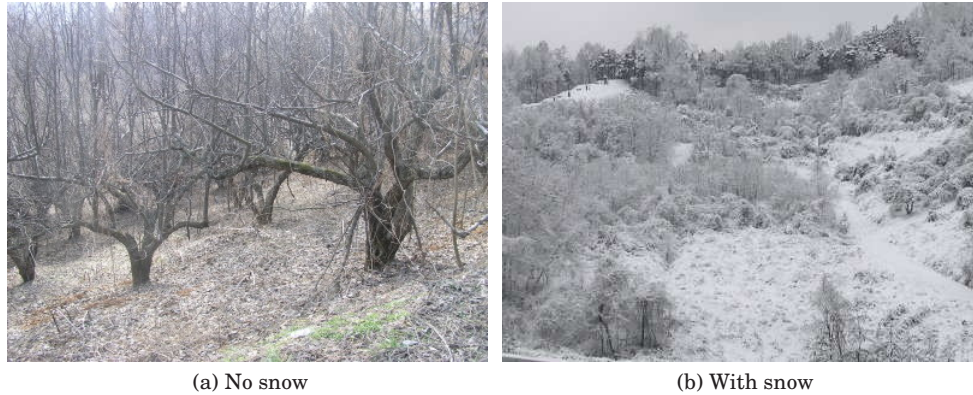
(a) No snow                                              (b) With snow

Fig. 2.   Location II

area of $0.72\text{m}^2$. A scan is performed by moving the receiver along a horizontal plane with the center of the plane normal to the transmitter's location at a speed of 0.48m/s (Fig. 3). Each scan area consists of 7 parallel lines separated by 10cm increments.

Consistent with previous works [Hoffman and Cox 1982; Cox et al. 1983], we use the measured signals' median level at each local area to characterise the large-scale path loss. The median and mean are stationary over a local area, but the median value is less affected in cases where part of the measured signal is below the noise floor.

For irregular terrain, each scan line followed the contours of the terrain at a fixed height while maintaining an upright antenna position for the receiver. This raster scanning technique has been shown by [Hoffman and Cox 1982] to produce results very similar to those performed by mechanical devices with no human intervention.

### 3.4. Channel Pathloss Models

To model large-scale path loss for wireless communications, the free space, two-ray ground reflection, and log-distance models [Rappaport 2001] are the most widely used. However, for surface-level propagation, we need to take into account the effects of the surface wave. We compare our measurements results against all these models to determine a suitable path loss model for surface-level WSNs. While the free space, two-ray ground reflection, and ground-wave models predicts the path loss given environmental and system parameters, we use our measurement results to estimate the least squares error (LSE) path loss exponent $n$ and standard deviation $\sigma_{dB}$ for the log-distance and log-normal models.

The *free space* model predicts the received signal strength when the first Fresnel zone between a transmitter-receiver (T-R) pair is clear of obstacles. The free space received power (in mW) is a function of the distance $d$ between the pair and is obtained from the Friss free space equation below [Rappaport 2001],

$$P_0(d) = \frac{P_t G_t G_r \lambda^2}{(4\pi)^2 d^2 L} \tag{1}$$

where $P_t$ is the transmitted power in mW, $G_t$ and $G_r$ are the transmitting and receiving antenna gains, respectively, $\lambda$ is the wavelength of the signal, and $L$ is the system path loss. A summary of the mathematical notations used here and in the following sections are given in Table I.
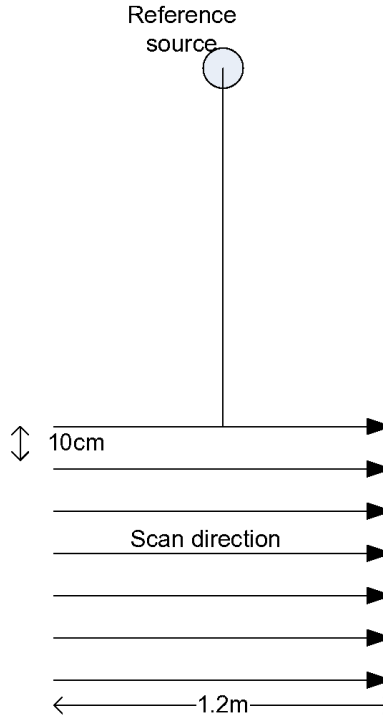
Fig. 3.   Raster scan pattern

A fundamental space field intensity $E$ equation arising from the effects of plane earth on the propagation of radio waves is given by [Bullington 1947] as

$$\frac{E}{E_0} = \overbrace{1}^{\text{Direct wave}} + \overbrace{\Gamma e^{j\Delta}}^{\text{Reflected wave}} + \overbrace{(1-\Gamma)Ae^{j\Delta}}^{\text{Norton surface wave}} \tag{2}$$

where $\Gamma$ is the ground reflection coefficient, $\Delta$ is defined in Table I, $E_0$ is the free space field intensity in units of volts per meters (V/m):

$$E_0 = \frac{\sqrt{30P_tG_t}}{d} \tag{3}$$

and $A$ is the surface wave attenuation factor:

$$A \approx \frac{-1}{1 + j\frac{2\pi d}{d}(sin\theta + z)} \tag{4}$$

The three components of this field make up the *ground-wave*. The relationship between $E$ and the received power is:

$$P_r(d) = P_0 \left| \frac{E}{E_0} \right|^2 \tag{5}$$

When both antennas are elevated at least one $\lambda$ above ground (or 5-10 $\lambda$ over water), the Norton surface wave attenuation factor can be ignored and (2) reduces to:

$$\frac{E}{E_0} = 1 + \Gamma e^{j\Delta} \tag{6}$$

Table I. Mathematical Notations

| | |
|---|---|
| $P_r$ | Received power (mW) |
| $P_t$ | Transmitted power (mW) |
| $P_0$ | Received power in free space (mW) |
| $G_r$ | Receiver antenna gain |
| $G_t$ | Transmitter antenna gain |
| $d$ | Transmitter-Receiver separation distance (m) |
| $\lambda$ | Wavelength (m) |
| $L$ | System loss factor not related to propagation |
| $h_r$ | Receiving antenna height (m) |
| $h_t$ | Transmitting antenna height (m) |
| $\overline{PL_{dB}}(d)$ | Mean path loss (dB) as a function of distance |
| $d_0$ | Reference distance (m) |
| $n$ | Pathloss exponent |
| $E$ | Electric field intensity (V/m) |
| $E_0$ | Electric field intensity for free space (V/m) |
| $A$ | Surface wave attenuation factor |
| $\Gamma$ | Ground reflection coefficient |
| | $\Gamma_\parallel = \frac{\epsilon \sin\theta - \sqrt{\epsilon - \cos^2\theta}}{\epsilon \sin\theta + \sqrt{\epsilon - \cos^2\theta}}$ (Vertical polarisation) |
| | $\Gamma_\perp = \frac{\sin\theta - \sqrt{\epsilon - \cos^2\theta}}{\sin\theta + \sqrt{\epsilon - \cos^2\theta}}$ (Horizontal polarisation) |
| $z$ | $z_\parallel = \frac{\sqrt{\varepsilon - \cos^2\theta}}{\varepsilon}$ (Vertical polarisation) |
| | $z_\perp = \sqrt{\varepsilon - \cos^2\theta}$ (Horizontal polarisation) |
| $\theta$ | Grazing angle - angle between reflected ray and ground(º) |
| $\varepsilon$ | Complex relative permittivity |
| | $\epsilon - j60s\lambda$ |
| $\epsilon$ | Dielectric constant of ground relative to unity in free space |
| $s$ | Conductivity of ground (mhos per meter) |
| $\Delta$ | Phase difference between direct and reflected E-field components $\approx \frac{4\pi h_t h_r}{\lambda d}$ |
| $h_0$ | Minimum effective antenna height (m) |
| $X_{\sigma_{dB}}$ | Zero mean Gaussian distributed random variable with standard deviation $\sigma$ (both in dB) |
| $\sigma$ | Standard deviation |

The predicted reception power using this field intensity equation is known as the *two-ray ground reflection* model and can be derived from (5) and (6):

$$P_r(d) = \frac{P_t G_t G_r}{L} \left( \frac{\lambda}{4\pi d} \right)^2 |1 + \Gamma e^{j\Delta}|^2 \tag{7}$$

For near grazing paths, $\Gamma$ is approximately -1 for both horizontal and vertical polarization. This reduces (7) to:

$$P_r = \frac{P_t G_t G_r}{L} \left( \frac{\lambda}{4\pi d} \right)^2 |2sin\frac{\Delta}{2}|^2 \tag{8}$$

When $\Delta/2 < \pi/10$, $sin\frac{\Delta}{2} \approx \frac{\Delta}{2}$. Thus, for $d > (20h_t h_r/\lambda)$, the two-ray ground reflection model can be simplified to:

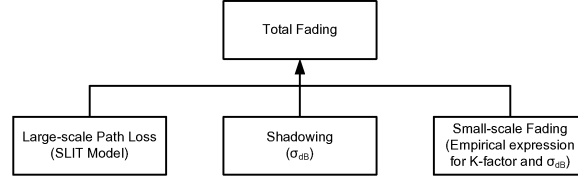$$P_r(d) = \frac{P_t G_t G_r}{L} \frac{h_t^2 h_r^2}{d^4} \tag{9}$$

Fig. 4.   Overview of Model and Contribution

and this equation is used in network simulators such as [NS2 2009; Qualnet 2009]. For conditions when $d < (20h_t h_r/\lambda)$, the received power theoretically oscillates between local maxima of 6dB above free space to $-\infty$dB at local minima. Both [NS2 2009; Qualnet 2009] use (1) to approximate the path loss at this range for simplicity.

When antennas are located near ground ($h_{r,t} < \lambda$), the first two terms in (2) cancel each other out ($\Gamma \approx -1$ and $h_{r,t} \approx 0 \therefore \Delta \approx 0$). The surface wave thus becomes a more dominant component of the signal propagation mechanism. The magnitude of the third term in (2) can be written as [Bullington 1947]:

$$|(1 - \Gamma)A| \approx \frac{2}{\frac{2\pi d}{\lambda} z^2} = \frac{4\pi h_0^2}{\lambda d} \tag{10}$$

where $h_0$ is the minimum effective antenna height:

$$h_0 = \left| \frac{\lambda}{2\pi z} \right| \tag{11}$$

Using (1), (5) and (10), we simplify the *surface wave* path loss model as:

$$P_r(d) = \frac{P_t G_t G_r}{L} \left( \frac{h_0}{d} \right)^4 \tag{12}$$

which is similar to (9) except for the change in the minimum effective antenna height.

The *log-distance* path loss model predicts the average path loss for a T-R separation based on the measured path loss at a reference distance $d_0$ and a given path loss exponent $n$, both of which are usually obtained from experimental results. In Appendix B, we report the best fit for $n$ from our measurement results, estimated using LSE, for the equation given in [Rappaport 2001]:

$$\overline{PL_{dB}}(d) = \overline{PL_{dB}}(d_0) + 10n \log \frac{d}{d_0} \tag{13}$$

Due to various objects in the environment, two different locations with the same T-R separation may have a large difference in received signal strength. Measurements from [Cox et al. 1983] have shown that the median path loss for any small-scale area with a T-R separation of $d$, is log-normally distributed about the mean value predicted by (13). This *log-normal shadowing* model is given as [Rappaport 2001]:

$$PL_{dB}(d) = \overline{PL_{dB}}(d_0) + 10n \log \frac{d}{d_0} + X_{\sigma_{dB}} \tag{14}$$

where $X_{\sigma_{dB}}$ is a zero-mean Gaussian distributed random variable with a standard deviation $\sigma_{dB}$, both in dB. We also present the value of $\sigma_{dB}$ from our measurement results in Appendix B.

Fig. 4 shows a brief overview of our model and contributions that will be detailed in the following sections. We show that the ground-wave and surface wave models can accurately model the path loss in flat terrain (Sec 4.1), and present the surface-level
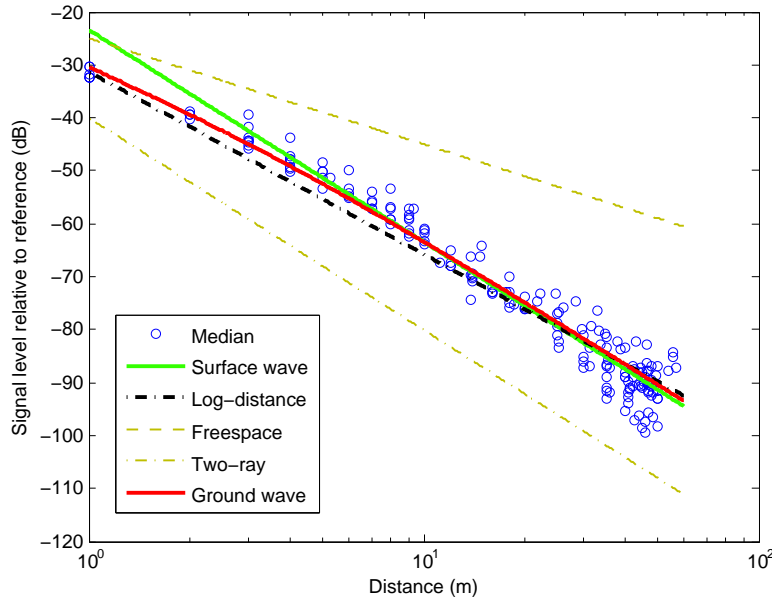
Fig. 5.   Measured signals' median levels relative to reference at Location I

irregular terrain (SLIT) model that takes into account the path profile and effective antenna height for large-scale path loss prediction in irregular terrain (Sec 5.2). The contributions of shadowing are reported as the standard deviation $\sigma_{dB}$ for a log-normally distributed random variable for the SLIT model for flat and irregular terrain (Sec 4.1, 5.1, 5.2). We also show that the small-scale area fading is Rician distributed, and we propose an empirical expression of the average K-factor based on the distance from the signal source and report the standard deviation $\sigma_{dB}$ for a log-normally distributed random variable around the average K-factor (Sec 4.2, 5.3). Finally, all three different effects are combined as the distance and terrain dependent total fading experienced at a randomly positioned receiver (Sec 4.3, 5.4).

## 4. FLAT TERRAIN

### 4.1. Large-scale path loss

The data points in the log-log graph in Fig. 5 are the median values of the signal envelope from scans recorded in various randomly selected positions in Location I. The signal levels in the y-axis of the figure is relative to the transmitter's measured output. The free space (1) and two-ray (7) models severely under- and overestimate the actual path loss, respectively, for the given measurement parameters ($h_{r,t} = 0.1, d >> (20h_t h_r/\lambda)$). Detailed results for the log-normal shadowing model are available in Appendix B.

The simplified surface wave path loss model (12) gives a very good prediction of the actual path loss for distances farther than 3-4m from the signal source at Location I for $\epsilon = 3.9$ and $s = 0.058$, both estimated using a technique proposed in [Kim and Narayanan 2002], and vertical antenna polarisation. The reason for the error at closer distances is because the direct and reflected wave terms do not completely cancel each other out (i.e. $\Gamma > -1$). For these distances, the more complicated ground-wave model (2) gives a very accurate result. The ground-wave model predicts the slower rate of decay for signals at closer distances before a steeper slope further away from the signal
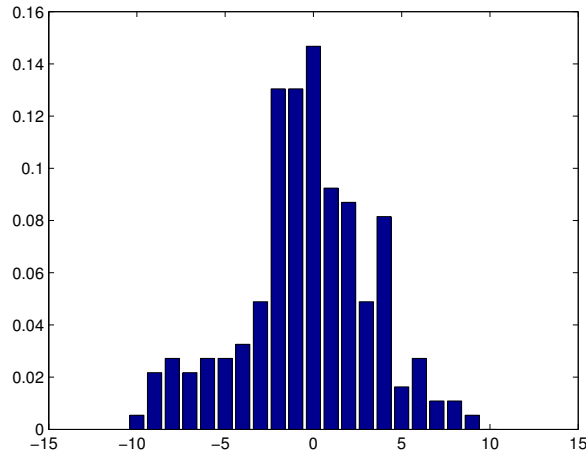
Fig. 6. Probability distribution of signals' medians around predicted path loss ($d > 3$m)

source that matches the simplified surface wave path loss model. Results from Location III match those from Location I when the ground-wave or surface wave models are used with measured $\epsilon = 5.6$ and $s = 0.036$. We speculate that the effects of the direct and reflected waves at closer distance along with the surface wave component probably accounts for the "2-slope" result observed in [Martfnez-Sala et al. 2005] as well.

In Fig. 6, we plot the histogram of the signal envelope medians after removing the surface wave trendline for distances 3m and above from the reference source. We can see that the distribution tends to be log-normal with a $\sigma_{dB}$ of 3.67. As such, the received median signal strength for a random small-scale area with T-R separation $d$ can be modelled using the simplified surface wave model (12) as:

$$P_{r_{fl1}(dBm)}(d) = 10 \log \left( \frac{P_t G_t G_r}{L} \left( \frac{h_0}{d} \right)^4 \right) + X_{\sigma_{dB}} \tag{15}$$

where $X_{\sigma_{dB}}$ is a Gaussian distributed random variable with a standard deviation of $\sigma_{dB}$, both of which are in dB.

We would like to highlight that (15) gives a very accurate prediction of the mean large-scale path loss for distances after the inflection point using just the $\epsilon$ and $s$, which can be obtained using simple techniques proposed in [Kim and Narayanan 2002] (a caveat to this method not mentioned in the paper is that measurements for lower frequencies are best performed with smaller incidence angles or to use higher frequency signals for better accuracy). If accurate prediction of path loss for small T-R separation is needed, the ground wave model (2) can be used together with the measured $\epsilon$ and $s$. The alternative method to model the received signal strength is to employ extensive measurements to find the best fit $n$ for the log-distance model and also the inflection point where $n$ shifts to a deeper gradient.

## 4.2. Small-scale Fading

Fig. 7 shows the signal level for each raster scan line at a position 30m away from the signal source at Location I. This figure is representative of scans far from the signal source. Due to multipath propagation, even static nodes located relatively near each other can experience significant fading effects. In conditions when the LOS path between a T-R pair is totally obstructed, the fading is normally characterised as a Rayleigh distribution [Hoffman and Cox 1982; Cox et al. 1983]. In this subsection, we try to fit the small-scall fading effects measured at Location I, where half of the first
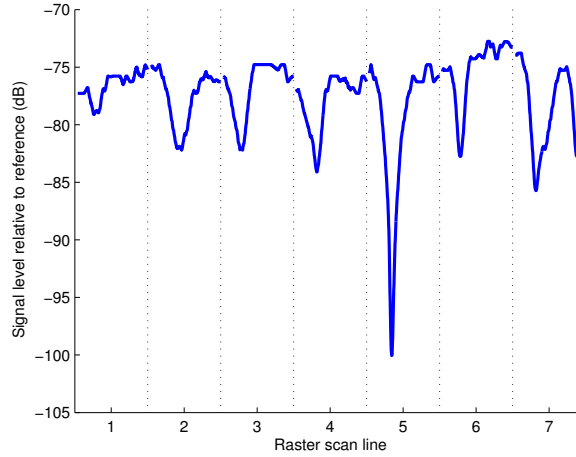
Fig. 7.   Signal scan at 30m from the source

Table II. Average RMSE for each distribution

| Distribution | Rice | Rayleigh | Gaussian | Extreme Value |
|---|---|---|---|---|
| RMSE (all) | 0.0556 | 0.0807 | 0.0557 | 0.0581 |
| RMSE ($<$10m) | 0.0673 | 0.0918 | 0.0675 | 0.0695 |
| RMSE ($\geq$10m) | 0.0454 | 0.0707 | 0.0454 | 0.0481 |

| Distribution | Weibull | LogNormal | Nakagami |
|---|---|---|---|
| RMSE (all) | 0.0639 | 0.0598 | 0.0565 |
| RMSE ($<$10m) | 0.0707 | 0.0690 | 0.0675 |
| RMSE ($\geq$10m) | 0.0571 | 0.0516 | 0.0467 |

Fresnel zone is blocked by the surface, with the Rice, Rayleigh, LogNormal, Gaussian, Weibull, Nakagami, and Extreme Value distributions[Parsons 1992]. All of these distributions have been used to characterise small-scale fading in wireless networks.

From the measured signal power, we extract the voltage amplitude of the received signals envelopes for each scanned area, and normalise it to the median. We then used the normalised values for distribution fitting. Table II shows the root mean square error (RMSE) between the theoretical distributions and measurement results. A smaller RMSE shows a better fit for the distribution [Hashim and Stavrou 2005]. The Gaussian and Rician distribution shows the best fits for the small-scale fading in Location I. Since the Rician distribution is generally used to model small-scale fading with a dominant path, we will use it to analyse our results.

The Rician probability density function is given as [Abdi et al. 2001]

$$f_R(r) = \frac{2(K+1)r}{\Omega} e^{(-K - \frac{(K+1)r^2}{\Omega})} I_0\left(2\sqrt{\frac{K(K+1)}{\Omega}}r\right), r, K, \Omega \geq 0 \tag{16}$$

where $I_0(\cdot)$ is the zeroth-order modified Bessel function of the first kind, and $K$ and $\Omega$ are the shape and scale parameters, respectively. $K$ is the ratio of the power received via the dominant path to the power contribution of the random paths, and $\Omega = E[R^2]$ is the average signal power, where $R(t)$ is the received signal envelope. Since the voltage level was normalised about the median, $K$ completely specifies the fading distribution. We used the moment method [Abdi et al. 2001] to estimate $K$ from our measurement.

(a) K-factor (dB) versus distance (m)

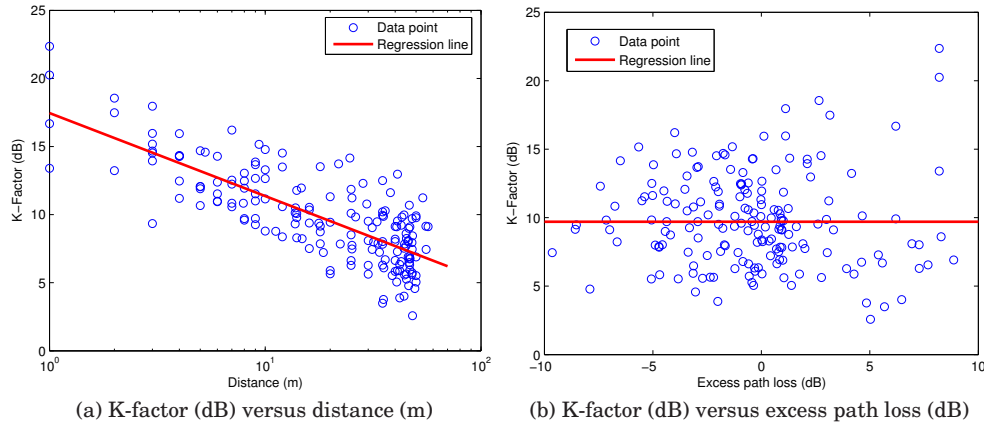(b) K-factor (dB) versus excess path loss (dB)

Fig. 8. Factors in determining Rician K-factor

Fig. 8a shows the plot of the measured Rician K-factor in dB ($K_{dB}$) versus the distance in log scale from the signal source. The LSE regression line shows a strong negative correlation between $K_{dB}$ and distance. The $K_{dB}$ is found to be normally distributed around the regression line with a standard deviation $\sigma_{dB}$ of 2.13dB. Therefore we propose the following equation to model the K-factor as a function of distance

$$K_{dB}(d) = C_1 \log(d) + C_0 + X_{\sigma_{dB}}$$

$$\text{or} \tag{17}$$

$$K(d) = d^{\frac{C_1}{10}} 10^{\frac{C_0 + X_{\sigma_{dB}}}{10}}$$

$$\tag{18}$$

where $C_1 = -6.09$ and $C_0 = 17.46$ are the coefficients for Location I, and $X_{\sigma_{dB}}$ is a Gaussian distributed random variable.

Fig. 8b plots the measured $K_{dB}$ versus excess path loss in decibel ($EPL_{dB}$). Excess path loss here is defined as the measured path loss minus the theoretical mean path loss. This means that the higher the $EPL_{dB}$, the lower the measured signal is relative to the predicted mean path loss. Results shown here use (12) for the predicted mean path loss. For $d \geq 3$m, results from (13) are quite similar to those of (12) and will not be shown here. From Fig. 8b, we can see that there is negligible correlation between $K_{dB}$ and $EPL_{dB}$.

The correlation matrix for $\log(d)$, $EPL_{dB}$, and $K_{dB}$ is given below:

$$\boldsymbol{\rho}(\log(d), \boldsymbol{EPL_{dB}}, \boldsymbol{K_{dB}}) = \begin{bmatrix} 1.0000 & -0.0122 & -0.7013 \\ -0.0122 & 1.0000 & -0.0150 \\ -0.7013 & -0.0150 & 1.0000 \end{bmatrix} \tag{19}$$

Results for the K-factor coefficients from Location III, which is also a flat terrain, is quite similar to those from Location I although the ground quality is slightly better (larger value of $\epsilon$), and we do not factor in the ground conditions here. However, it might have to be considered for larger differences in $\epsilon$, and more experiments are required in the future for different ground types to determine this. Temporal changes to ground conditions due to weather (i.e. rain and snow) were found to have negligible effects.
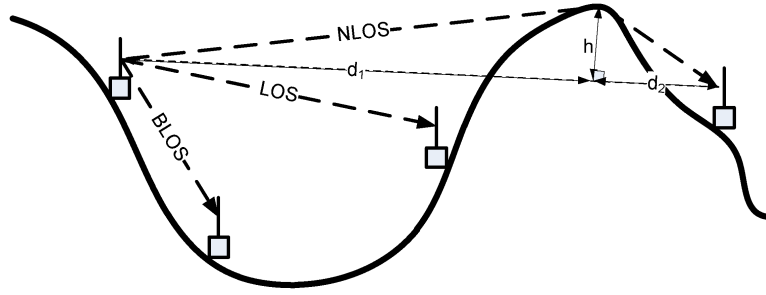
Fig. 9.   Classification of paths

## 4.3. Summary

The results above show that the path loss for any T-R pair located at surface-level on a flat terrain is a random value. The large-scale path loss can be modelled using (15) as a log-normally distributed value about a distance-dependent mean. This value is also the median of the signal strength received within a small-scale area, which is Rician distributed with a distance dependent K-factor (18). From (15) and (18), the received signal power in dBm for a T-R pair with separation of $d$ can be modelled as

$$P_{r_{fl2}(dBm)}(d) = P_{r_{fl1}(dBm)}(d) + 20\log(R(K(d))) \tag{20}$$

where $R(K(d))$ is a Rician random variable.

The received power calculated from (14) can also be used in place of (15) in the equation above if a log-normal shadowing model is used.

## 5. IRREGULAR TERRAIN

### 5.1. Large-scale path loss

For irregular terrain, we classify measured signals according to three types of path profiles; these paths are line-of-sight (LOS), blocked LOS (BLOS), and non-LOS (NLOS) paths as shown in Fig. 9. LOS refers to paths that have a significant clearance above ground and no obstacles in between the T-R pair, although in most cases for nodes on surface-level, there is a probability that the edges of the first Fresnel zone for UHF signals will be infringed upon by external objects since the size of the Fresnel zone is large. BLOS paths are for T-R pairs that are located along the same incline with no significant obstacles or depression (clearance) in-between, which means that almost half of its Fresnel zone is obstructed by the ground. NLOS paths occur when the nodes are completely blocked from each other by a large obstacle, with a diffracted signal arriving at the receiver or in other words, the Fresnel zone is almost completely obstructed. These classifications serve as a rough guide as there are many borderline locations that may be described as either one of two different types of paths.

The data points in Fig. 10 are the median small-scale area signal levels at various points in Location II. The surface wave and ground-wave lines are based on the estimated $\epsilon$ of the location (which is located near Location I and has a slightly higher $\epsilon = 4.3$). The linear regression line is the LSE fit for all the sample points. From the results, (12) and (2) show a very good fit for the BLOS data similar to the flat terrain. However, the data points for LOS and NLOS paths show a large deviation from the predicted value. The standard deviation for all the data points from the model trendline is 9.64dB. The standard deviation for the surface wave model is similar to the ground-wave model for $d > 3$m.
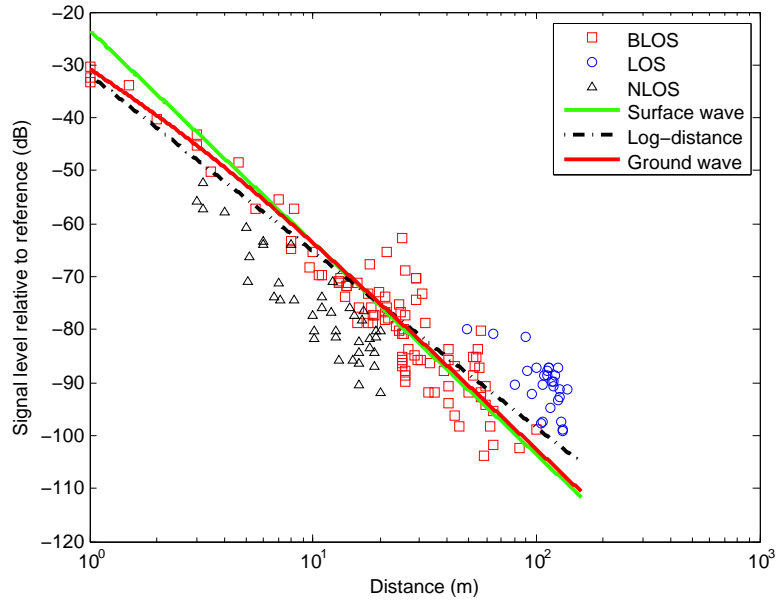
Fig. 10.   Measured signals' median levels relative to reference at Location II. The average standard deviation of the measured signals is 2.93dB.
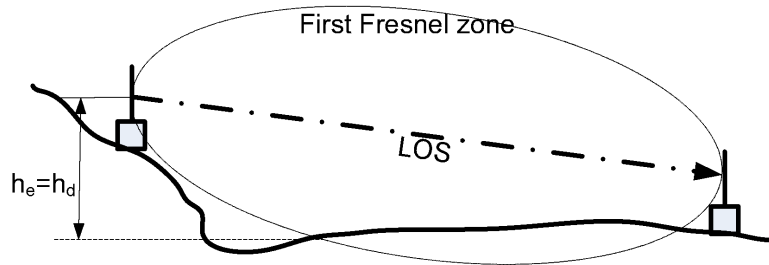


Fig. 11.   Effective antenna height

### 5.2. Surface-Level Irregular Terrain (SLIT) Model

To model the path loss for the LOS paths more accurately, we found the difference in height $h_d$ between the transmitting antenna and the point where the first Fresnel zone intercepts the terrain to be a suitable effective antenna height (Fig. 11) to use. The RMSE between the measured path loss for LOS data and the predicted path loss using (12) is 15.46dB. By applying the new effective antenna height, the RMSE between the measured LOS data and the new predicted path loss becomes 3.92dB. Substituting the new effective antenna height into (12), the received signal strength for LOS paths can then be modelled as follows:

$$P_{r_{ir1}}(d) = \frac{P_t G_t G_r}{L} \left( \frac{(h_d h_0)}{d^2} \right)^2 \tag{21}$$

Fig. 12 shows the excess path loss from the measured signals relative to the surface wave model (12) (and subsequently, ground-wave). As can be seen, the surface wave
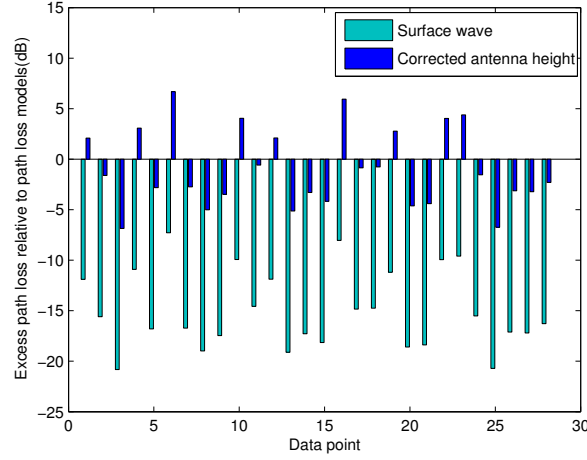
Fig. 12.   Excess path loss for LOS paths

model severely underestimates the path loss compared to the measured LOS data. Using (21), a more accurate prediction of the path loss can be obtained when there is partial clearance around the transmitter.

For NLOS paths, we find that we can use a knife-edge model to represent the obstacles and the classical Fresnel solution to obtain a relatively accurate path loss model if there is a sharp bend along the surface path between the T-R pair with angle $\alpha$ (Fig. 13). From our experimental results, when $\alpha \geq 35°$ and the path then continuing at least $\lambda$ in the same direction, additional diffraction gains $G_d$ have to be accounted for. For NLOS paths with only gradual changes along the path, the signal seems to be guided along the surface and no additional diffraction gains occur. $G_d$ can be obtained using the terrain information to calculate the Fresnel-Kirchoff diffraction parameter $v$ [Parsons 1992]

$$v = h\sqrt{\frac{2(d_1 + d_2)}{\lambda d_1 d_2}} \tag{22}$$

where $h, d_1$, and $d_2$ are in terms of the geometry of Fig. 9. Instead of solving for the complex Fresnel integral [Parsons 1992], $G_d$ can then be approximated using the equations derived from [Lee 1982]

$$G_d(v) = \begin{cases} 0.5 - 0.62v & -0.8 < v < 0 \\ 0.5e^{-0.95v} & 0 < v < 1 \\ 0.4 - \sqrt{0.1184 - (0.38 - 0.1v)^2} & 1 < v < 2.4 \\ \frac{0.225}{v} & v > 2.4 \end{cases} \tag{23}$$

The diffraction gain is then included into (14) to predict the mean received signal strength as below

$$P_{r_{ir1}}(d) = G_d^2 \frac{P_t G_t G_r}{L}\left(\frac{h_0}{d}\right)^4 \tag{24}$$

$G_d^2$ is used because $G_d$ is calculated from volts instead of watts. Fig. 14 compares the excess path loss predicted using (12) and (24). A much more accurate path loss
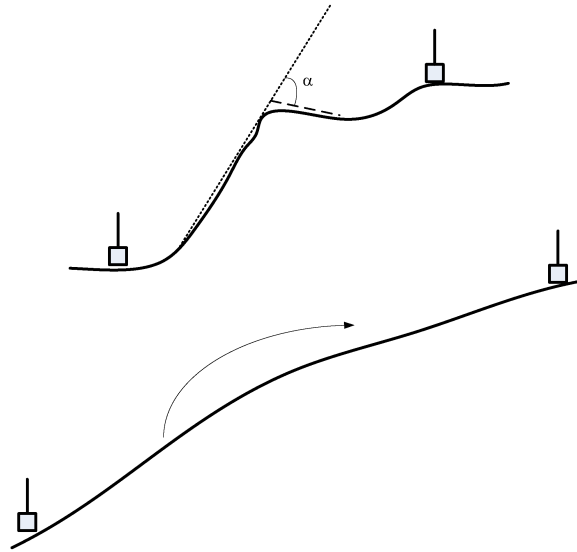
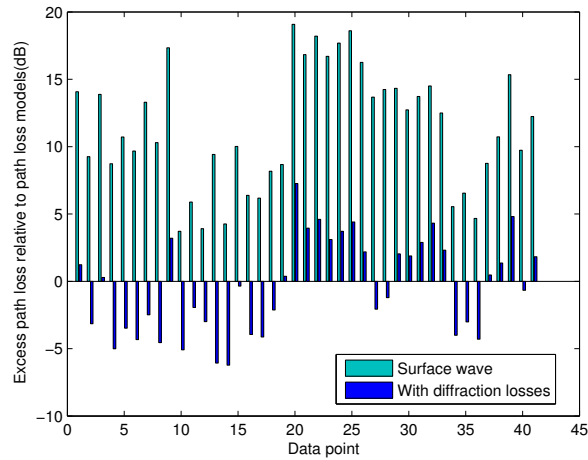Fig. 13.   NLOS paths with sharp bend (top) and gradual change (bottom)



Fig. 14.   Excess path loss for NLOS paths

prediction is obtained after including the diffraction gain into the results. The RMSE with and without diffraction gain is 3.25 and 12.66 dB, respectively.

We propose the following surface-level irregular terrain (SLIT) model to calculate the large-scale mean path loss for any given T-R pair at surface-level on irregular terrain through the following steps:

(1) Determine the larger of $h_0$ and $h_d$ to be used as the effective transmitting antenna height.
(2) Using the original antenna geometry, determine if there are any additional features in the path profile that can cause additional diffraction gains using the DEM information.
    — First determine the distance between the T-R pair in a straight path.

— Then, perform a search using the DEM data for the terrain peak between the T-R pair to determine if it obstructs the LOS of the T-R pair and if there is a sharp bend at the peak as shown in Fig. 13.

— If both of these conditions are met, calculate the height of the obstacle as the perpendicular distance from the top of the obstacle to the direct line between the T-R pair (Fig. 9). The distance between the intersection of the two lines and T is denoted as $d_1$ and the distance between the intersection and R is denoted as $d_2$. Using these values, calculate $v$ for the path from (22) and use it to find $G_d$ from (23).

(3) Calculate the average received power using the following equation obtained from combining (12), (21), and (24):

$$P_{r_{ir1}}(d) = G_d^2 \frac{P_t G_t G_r}{L} \left( \frac{h_d h_0}{d^2} \right)^2 \tag{25}$$

Using this proposed method, most of the outliers classified as BLOS can be more accurately modelled. For example, the RMSE between the measured value and the predicted path loss for the six BLOS data points above the linear regression line at distances of 20-30m in Fig. 10, is 2.39 and 12.48 dB for the SLIT model and the simplified surface wave model, respectively.

Finally, the median received power for a random small-scale area in irregular terrain with a T-R separation of $d$ can be represented as

$$P_{r_{ir1}(dB)}(d) = 20 \log \left( G_d \left( \frac{h_d h_0}{d^2} \right) \right) + 10 \log \left( \frac{P_t G_t G_r}{L} \right) + X_{\sigma_{(dB)}} \tag{26}$$

where $X_{\sigma_{(dB)}}$ is Gaussian distributed random variable with a $\sigma_{dB} = 4.38$.

We would like to note that there is no actual need to classify path profiles when using the SLIT model as the steps in SLIT already factors in both antenna height adjustments and diffraction losses on the path between a T-R pair based on the terrain's surface. This terrain-based path profile is then used to more accurately calculate the large-scale path loss rather than relying on either a log-distance path loss model with a single path loss exponent and a very large standard deviation or requiring multiple path loss exponents and having to determine when to apply one of it for a T-R pair, based on a classification of the path profile that can be arbitrary and inaccurate in many borderline cases.

### 5.3. Small-scale Fading

Using the method described in sub-section 4.2, we find that the Rician distribution gives the best fit for the small-scale fading in irregular terrain as well with a RMSE of 0.0521. Fig. 15a plots the estimated $K_{dB}$ from our measurements versus the distance from the signal source in log scale. Similar to the results measured on the flat terrain, the graph suggests that $K_{dB}$ is negatively correlated to the distance from the sender.

Fig. 15b shows the estimated $K_{dB}$ versus the excess path loss between the measurement results and the SLIT model. Similar to the flat terrain, there is no correlation between the excess path loss and the K-factor. Therefore, (18) can be used for irregular terrain as well, with $C_1 = -3.84$, $C_0 = 10.32$, and $\sigma_{dB} = 4.33$.

### 5.4. Summary

Similar to flat terrain, the received signal strength for a T-R pair at any given location in irregular terrain can also be modelled as a combination of two random variables. (26) models the large-scale path loss as a log-normally distributed value around a distance- and terrain-dependent mean calculated using the SLIT model (25). The small-scale

(a) K-factor (dB) versus distance (m)          (b) K-factor (dB) versus excess path loss (dB)
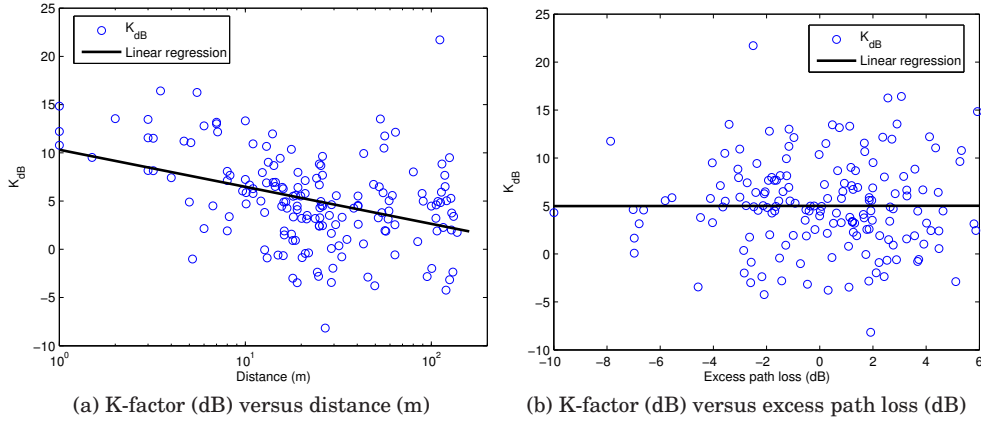
Fig. 15.   Factors in determining Rician K-factor

area fading in that particular location can then be modelled as a Rician distribution with a distance-dependent K-factor that can be obtained from (18). Combining (26) and (18), we can model the path loss for a particular T-R pair in irregular terrain as:

$$P_{r_{ir2}(dBm)}(d) = P_{r_{ir1}(dBm)}(d) + 20\log(R(K(d)))  \tag{27}$$

where $R(K(d))$ is a Rician random variable.

## 6. VERIFICATION OF PATH LOSS MODEL

To verify our proposed path loss model (25), we obtained high resolution 1m x 1m DEM (Digital Elevation Model) files from the Korean National Geographic Information Institute for an area near Location II, but with slightly steeper slopes. We then measured the gains of two $\lambda/4$ whip antennas at specific angles. To verify our results in irregular terrain, we measured the median small-scale area signal strength at 50 locations along 5 different paths (Fig. 16) with distances of between 20-65m from the signal source using the same methodology described in Section 3. We first coupled one of the whip antennas with the signal source. Next, we adjusted the antenna so that the angle with the known gain faced one of the 5 paths. Finally, we ensured that the angle of the antenna used for measurement of the signal strength faced the signal source to reduce differences caused by the difference in radiation pattern of the antennas while performing the raster scans. We repeated this procedure at each of the locations along every path.

After extracting the path profiles from the terrain information, we used the SLIT model to predict the signal strength at each location, and we compared the predicted values with our measurement results. The results show that the predicted received signal power is within ±8dB of the measured values (Fig. 17) and also within 2 standard deviations obtained from the previous results. The average difference between the measured results and the predicted results from the SLIT model is 2.56dB with a standard deviation of 1.82dB. The cumulative distribution function (cdf) of the difference between the measured and predicted values is plotted against the theoretical cdfs for the SLIT and log-normal (LN) models in Fig. 18. Some of the differences between the measured and predicted values could be attributed to shadowing by objects in the environment that are not part of the DEM information. One method to account for the additional shadowing could be by adapting RIM [Zhou et al. 2004] or other
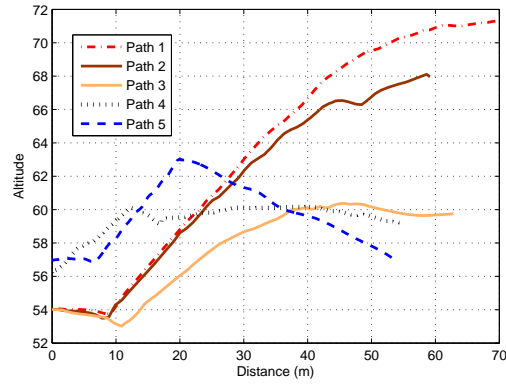
Fig. 16.   Path profile of irregular terrain verification site generated from DEM information
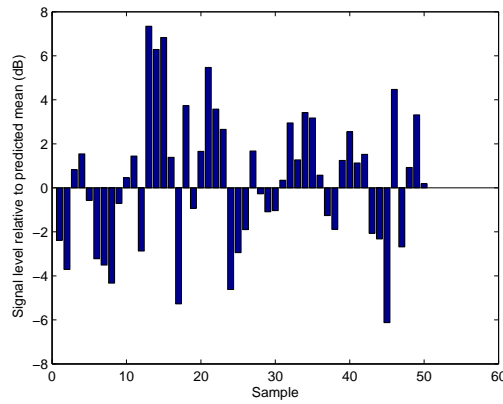


Fig. 17.   Measured signal level relative to predicted mean for irregular terrain verification location

Table III. Verification on flat terrain

| Location | $\epsilon$ | $s$ | $\sigma_{dB}$ |
|---|---|---|---|
| Park | 3.81 | 0.039 | 2.05 |
| Parking lot | 2.07 | 0.064 | 2.59 |
| River side | 6.13 | 0.012 | 2.18 |

similar models. However, there is significant work to be done for accurately modelling different objects in the environment, and we leave this for future work.

We also performed a similar verification on flatter terrain at a few different locations. Following the same techniques to measure the permittivity and conductivity of each location as described in [Kim and Narayanan 2002], we obtained the predicted mean large scale path loss at each site. Location with low $\epsilon$ are considered as poor ground where higher path loss will occur when RF signals are transmitted near the ground surface, while ground with higher $\epsilon$ cause less losses. We use the same antennas and technique to perform raster scans at 25 randomly chosen locations at each site between the distances of 20m-65m from the signal source, and compared the measured medians with the predicted average values. We ensured that there was no foliage or objects
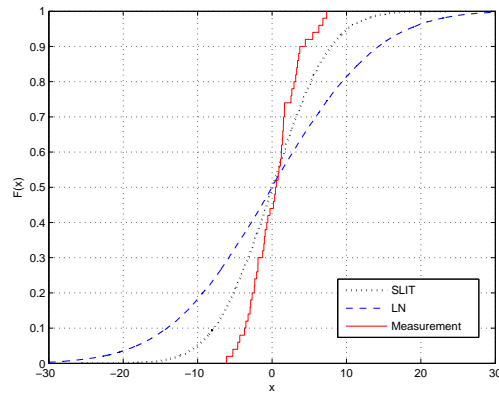
Fig. 18.   CDF of difference between predicted and measured path loss (Fig. 17)

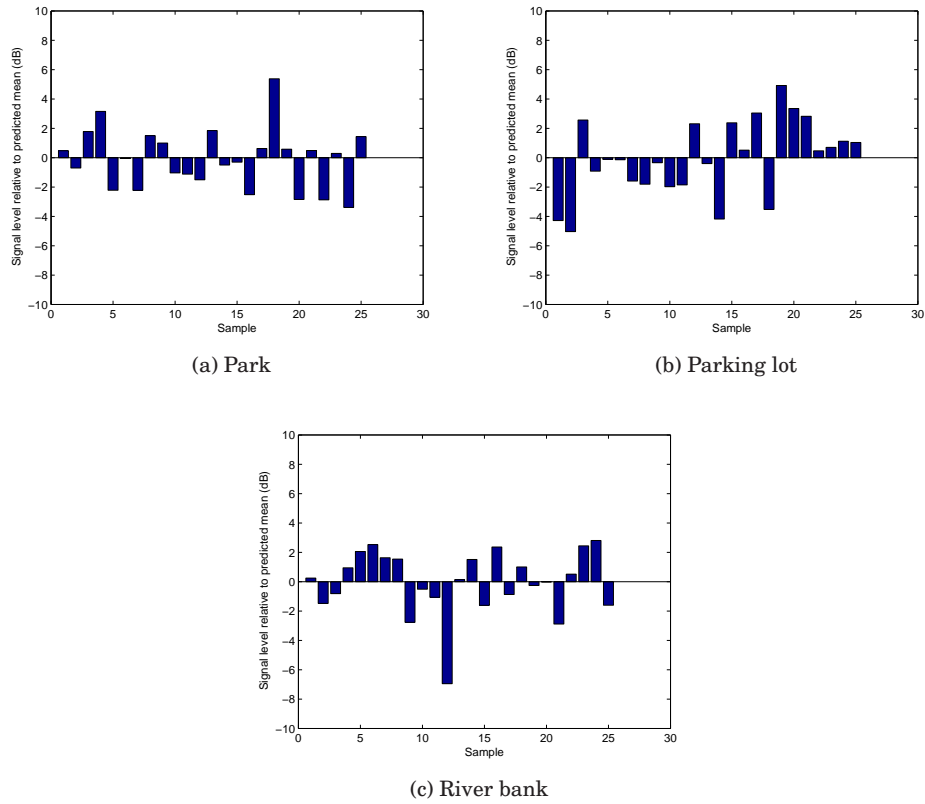

(a) Park



(b) Parking lot



(c) River bank

Fig. 19.   Measured signal level relative to predicted mean for different flat terrain

within the measurement locations that could cause additional path loss or small-scale fading that would affect the measurement results for each location [Chong et al. 2011]. The results are shown in Table III and Fig. 19. Most of the measured median values lie

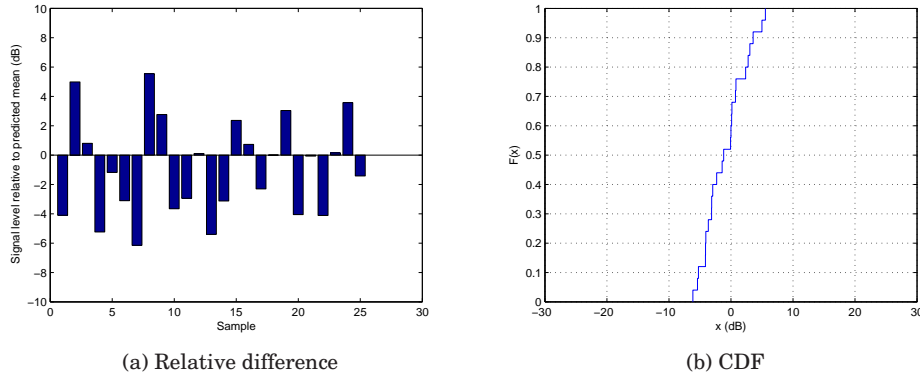(a) Relative difference                              (b) CDF

Fig. 20.   Measured signal level relative to predicted mean for 2.4GHz frequency band

within 2dB of the predicted values for all 3 sites. From the results obtained, it can be seen that using a model that includes the surface wave component gives an accurate prediction of path loss for sensor network communications located on different types of flat ground as well as irregular terrain for the 400MHz channel.

Using a similar method as above, we also attempted to verify the SLIT model using sensor nodes in the 2.4GHz band for irregular terrain. The results of the verification are shown in Fig. 20. The results show a slightly better performance compared to the 400MHz verification done on irregular terrain. The main reason for this is because the transmission ranges for 2.4GHz RF signals so close to the ground is much shorter than for the 400MHz band. Therefore, measurements for this frequency were performed closer to the transmitting antenna (between 10-35 m), and were less likely to be interfered with by objects in the environment unlike the previous verification for the 400MHz band performed over longer distances. The smaller Fresnel zones for 2.4GHz RF signals also mean that they are less likely to have interfering objects in the Fresnel zone, leading to smaller multipath effects compared to the 400MHz band for LOS propagation (less variation in a small-scale area).

We do not compare our results to other popular outdoor irregular terrain models such as Longley-Rice[Longley and Rice 1968], Edwards-Durkin[Edwards and Durkin 1969], and Egli [Egli 1957] models as they were proposed for propagation with antennas located higher than ground level. As such, they only consider the free space and two-ray propagation models, and tend to over predict the path loss for surface-level communications by not taking into account the surface wave component. Thus, we feel that such comparisons are inappropriate.

## 7. IMPACT OF THE SLIT MODEL

[Zhou et al. 2004; 2006] performed logical analysis and simulated the impact of irregular radio communications on existing MAC, routing, localization, and topology control protocols in wireless sensor networks. The impact of the results drawn from our work has many similarities with those of [Zhou et al. 2004; 2006] since our results show a slight variation in the placement of the radio within a small-scale area can result in a significant difference in static small-scale fading, while the radio signal strength received in different directions depends on the terrain between the transmitter and receiver. The main difference is that our work models the path loss using terrain information, which contributes to a portion of the radio communication irregularities
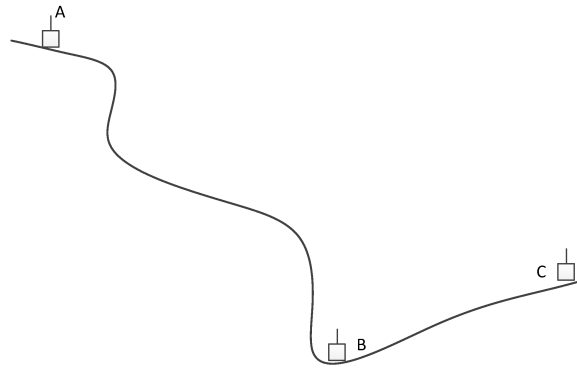
Fig. 21.   Hidden terminal problem and correlated path loss

observed previously. We discuss the additional impact that can be observed through the usage of the SLIT model below.

The irregularity of the communication range of sensor nodes in a 3-dimensional viewpoint does not just depend on the direction of the T-R pair; it also depends on the terrain between them. Consider the case shown in Fig. 21 where nodes B and C are in the same direction from node A. However, nodes A and B are hidden from each other due to the terrain profile, but are both exposed to node C. Situations such as this can lead to more collisions due to the hidden terminal problem, and are not commonly reflected in simulations. Since most sensor network MAC protocols use some form of carrier sensing to prevent collisions, evaluation using simulation with terrain profiles can help improve performance and parameter selection. Furthermore, some protocols which depend on nodes overhearing each others packets to resolve contention (for example, CMAC's [Liu et al. 2009] forwarding node contention protocol) may perform poorly in such environments.

Consider also the case where another node, D, is placed next to node C in Fig. 21. In the commonly used log-normal shadowing model, it is likely that the simulated path loss between the T-R pairs of A-C and A-D differ by a lot due to the randomly generated log-normal path loss variable. The non-correlation of received signal strength could lead to both nearby nodes having vastly different packet reception ratios. Another impact from irregular terrain that can be demonstrated by the SLIT model is that nodes that are located at the top of high ridges are likely to have much larger number of neighbouring nodes compared to nodes located at the bottom of slopes or in valleys. These highly elevated nodes are also more likely to be chosen by geographical forwarding algorithms [Karp 2000; Zorzi and Rao 2003; Liu et al. 2009] as forwarders since they are usually the furthest away from nodes at lower elevations. Due to their larger number of neighbours and more frequent requests to be forwarders, it is likely that the batteries of these nodes will drain off more quickly and suffer from more packet losses due to collisions. However, scenarios such as these may allow users new insight on ways to utilise geographical features for more efficient routing methods.

To highlight the differences between the SLIT model and commonly used path loss models, we use Qualnet [Qualnet 2009] to compare the performance of Geographic Forwarding (GF) [Karp 2000] and AODV [Perkins et al. 2003] over a simple duty-cycling CSMA MAC protocol modelled after X-MAC[Buettner et al. 2006] when using SLIT and the log-normal path loss model. We modelled the transceiver after TI's CC1101 [Texas Instruments 2008a] and we use a SINR model to determine the success of each packet reception event. In the simulation, we randomly place between 100 - 800 nodes within a 600m x 600m square area of irregular terrain obtained from the DEM map.

Table IV. Environmental & Physical Simulation Parameters

| | |
|---|---|
| Area | 600m x 600m |
| Number of nodes | 100 - 800 |
| Rx Sensitivity | -111dBm |
| Background noise | -105dBm |
| Tx Power | 10dBm |
| Phy header | 7Bytes |
| Phy footer | 2Bytes |
| ACK Packet | 4Bytes |
| Control Packet | 64Bytes |
| Data Packet | 64Bytes |
| Antenna height | 0.1m |
| Shadowing model | Log-normal (7.78dB) |
| Path loss exponent | 3.34 |
| Frequency | 433MHz |
| Packet reception | SINR model |
| Sensor range | 30m |
| # sensed objects | 3 |

The DEM data, which provides the longitude, latitude, and altitude in square grids for a given area, is used to derive the path profile between individual T-R pairs by using each nodes latitude and longitude coordinates to determine its position, and antenna elevation information to determine its height. The surface of the terrain along a T-R pairs path is extrapolated from the heights of the surrounding grid points and is used as the path profile. The SLIT model (Sec. 5.2) is then applied to each path profile to calculate the large-scale path loss between them. The calculation of the large-scale path loss can be either done before simulation or during run-time, if supported by the simulator. Precomputation results in faster simulation, but slower loading time, and requires a large number of values to be calculated and stored for mobile scenarios, while run-time computation results in large memory consumption during simulation. The large-scale path loss obtained from SLIT can also be used in conjunction with other path loss models such as foliage models and small-scale fading models for more detailed modelling.

We generate 3 events every second randomly across the map. Nodes within 30m of the event will generate a packet towards the sink. The log-normal path loss model disregards the effects of the terrain and uses parameters obtained from our measurements in Appendix B. To isolate the effects of the irregular terrain, we disregard the effects of the antenna radiation pattern and fast-fading in the environment here. However, these two effects can be easily used together with SLIT.

Fig. 22a shows the number of nodes that have connectivity to the sink, which we define as each hop to the sink along the route having a packet reception ratio of at least 0.1, when SLIT is used versus the log-normal model. The error bars in this figure show the maximum and minimum percentage of connected nodes measured over 30 simulations, while the large markers show the average measured value. As can be seen from the results, the percentage of nodes connected to the sink for the SLIT model is on the average lower than that of the log-normal model when the number of nodes in the network is small due to the effects of the terrain. However, it can be possible for the nodes in the SLIT model to have higher connectivity depending on the position of the nodes in the simulation. The large standard deviation in the results for SLIT is

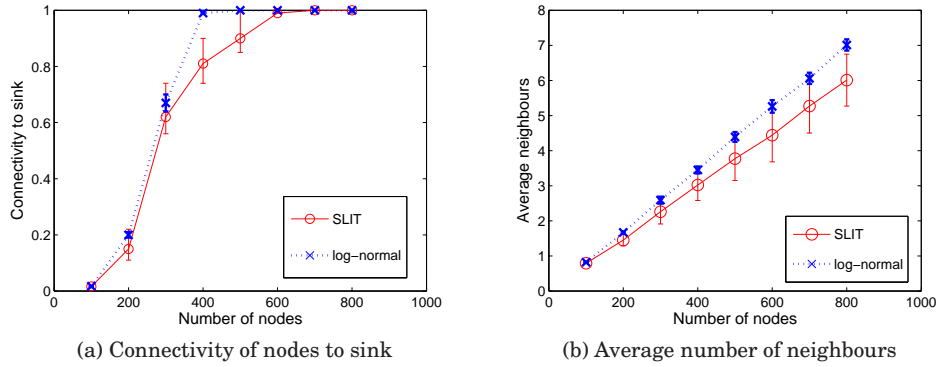(a) Connectivity of nodes to sink        (b) Average number of neighbours

Fig. 22.   Difference between SLIT and log-normal model

due to the random positioning of nodes. In scenarios where more nodes are located on elevated terrain, there is a higher chance that these nodes are able to communicate with a larger number of neighbours and serve as a link to the sink for other not so well connected neighbours. When most nodes are located in ravines or separated by geographical features, connectivity to the sink reduces due to the lack of candidate forwarders. This is a phenomenon that cannot be observed with the LN model due to the random assignment of shadowing values and the lack of correlation between neighbouring nodes, thus the connectivity of a node to the sink becomes a simple function of the node density in the network for the LN model.

Fig. 22b shows the average number of neighbours each node has depending on the density of the nodes in the network. On average, nodes in the SLIT model have lower number of neighbours compared to the log-normal model. However, the standard deviation (indicate by the error bars) of the number of neighbours each node has is also much larger in the SLIT model, due to the effects of the terrain elevation as mentioned above. This is an expected result based on our previous measurement which highlighted that nodes located on elevated terrain managed to transmit much further compared to nodes located on lower ground as long as there are no geographical obstructions. This translates to some nodes having a much larger number of neighbours compared to others. However, due to geographical features, the neighbours are usually distributed with a large bias towards certain directions. For the LN model, neighbours are usually distributed equally in all directions when the node density is high. This is also a factor that contributes to the higher connectivity seen in Fig. 22a.

While the preceding results highlight the difference between the SLIT model and the log-normal path loss model, Fig. 23a shows the impact of the irregular terrain on packet delivery. When actual terrain features are considered for path loss modelling, the AODV and GF protocols are shown to deteriorate drastically compared to when the terrain is "flattened". The sharp drop in the end-to-end packet delivery ratio for the GF protocol is mainly due to interference from hidden terminals as GF tends to select a node closest to the sink for forwarding. The signal strength for such T-R pairs are usually weak and are easily interfered from hidden terminals surrounding the pair. Furthermore, the GF algorithm is susceptible to void routes, which can easily occur in irregular terrain in the SLIT model, but is not seen in the log-normal path loss model. Another point of failure for GF which we found in our simulations is the tendency of neighbouring nodes to attempt to forward to the same elevated node on higher terrain due to the longer transmission distance achievable when SLIT is used.

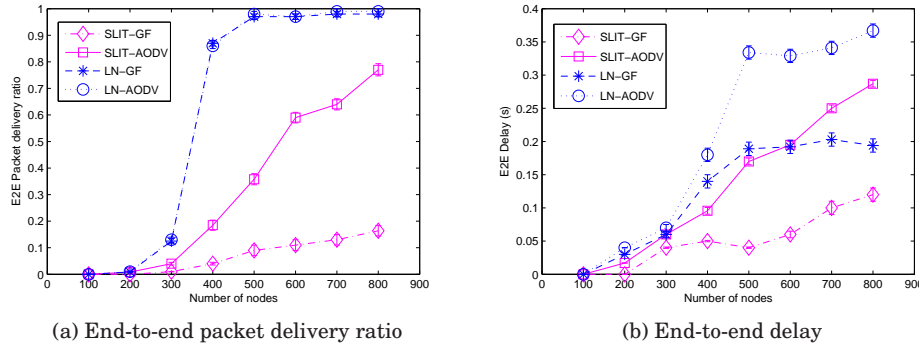(a) End-to-end packet delivery ratio             (b) End-to-end delay

Fig. 23.   Impact of SLIT model

This causes collisions at the receiver, especially when neighbouring nodes are unable to hear each other's transmission due to terrain features. The AODV protocol performs better than GF in irregular terrain due to its characteristic of finding multiple paths to the destination and its use of hops rather than distance as a routing metric.

The end-to-end delay for GF is generally lower than AODV due to it not requiring as many control packets and its greedy selection policy, which works well on flat terrain. In the case of when irregular terrain is taken into account, the packets that are delivered by GF are generally from nodes closer to the sink, thus skewing the delay metrics to a much lower value, while packets from nodes further away are mostly dropped along the way. The same is true for AODV in the SLIT model, but at a less inequitable scale, thus the observation that the end-to-end delay of SLIT-AODV being lower than LN-GF at certain lower node densities.

To summarise, the insights and additional information gained from using SLIT over the LN model from this simulation are:

— The number of neighbours that is within radio range not only changes depending on a node's location and path loss exponent, but may also be clustered in certain directions due to terrain factors.
— The node density needed to provide connectivity to the entire network depends more on the position of individual nodes for SLIT compared to the LN model, where a uniform path loss exponent and a random log-normal shadowing value that is assigned to T-R pairs ameliorates the effect of correlation between geographically co-located nodes.
— The performance of protocols can vary much greater in SLIT compared to the LN model due to geographical features influencing the RF propagation, thus making them more dependent on the location of neighbouring nodes, unlike the LN model that will average out when a larger number of neighbours are used. Geographical forwarding algorithms are more severely affected by irregular terrain compared to a reactive route discovery protocol like AODV, which performs better but at a cost of additional routing overhead.

Taking all these factors into account will be important for the simulation and deployment of real-world applications. The actual performance of the protocols and network life-time could be severely impacted compared to what is expected by the user if the LN model is used. We hope that the usage of SLIT will allow the development of protocols, through simulation, that will give a performance close to what is experienced in the real-world.

## 8. CONCLUSION AND FUTURE WORK

In this paper, we present results of channel measurements for outdoor, surface-level RF communications for WSNs in both flat and irregular terrain. Based on these measurements, we characterise the channel for surface-level communications for static nodes, and also proposed a new semi-empirical path loss model for surface-level WSNs called the SLIT model. We then verified this model using detailed terrain information and computer simulation. We also discuss the impact of the SLIT model on existing protocols and how it will affect the characteristics of simulation models. Finally, we discussed and performed simulations to highlight the impact of the more realistic SLIT model on sensor network simulations.

Key results show that it is necessary to include the direct, reflected, and surface wave components of a RF signal to accurately predict the large scale path loss for flat terrain. There is also a need to apply effective antenna heights and diffraction gains based on the path profile for more accurate path loss prediction in irregular terrain. Measurement results also show that fast fading in small-scale areas can be characterised as a Rician distribution with distance-dependent K-factor, and that significant differences in received signal strength can occur within small areas as the T-R separation increases.

The results and model presented here are also significant for sensor network applications such as localisation, simulation and modelling of protocols, or for deployment planning of sensor nodes in irregular terrain by providing a more accurate and realistic view of signal attenuation for surface-level WSNs communications.

Since there is a distinct lack of path loss models for surface-level wireless communications at the UHF band, we plan to perform more measurements and verification for other frequency bands and terrain in the near future to fine tune our work. Results from [Martínez-Sala et al. 2005] show path loss curves at a higher frequency (double that of the one used here) and at different locations that is consistent with what we have reported here. Therefore, we are confident that our proposed model can be extended to other frequency bands.

We would also like to explore ways to simplify our model to increase the ease of integration into existing network simulators such as ns-2[NS2 2009] for more accurate simulation results. As far as we know, ns-2 does not support small-scale fading models, while Qualnet uses two pre-generated sets of Gaussian random numbers to simulate Rayleigh or Rician fading. Qualnet also has a Longley-Rice based Irregular Terrain Model that we have modified to support SLIT.

Finally, we would like to highlight that while a lot of work has been done to characterise generic wireless communication channels [Andersen et al. 1995], a lot more work is needed to fully characterise surface-level propagation for different environments, such as urban, sub-urban, and indoor, that are likely to see sensor network deployment in the future. These characterisation includes path loss models, spatial fast-fading, and temporal fast-fading caused by environmental changes around static sensor networks.

## APPENDIX

### A. STANDARD DEVIATION OF MEASUREMENT SAMPLES

In this appendix, we present results for the standard deviation of each measurement sample taken at Location I and II. The graphs in Fig. 24 shows that the standard deviation tend to increase as distance increases. However, LOS and NLOS conditions (Fig. 24b) are also a factor in determining the standard deviation of the measurements as NLOS conditions means that there is no single dominant path between the T-R pair. This causes a multipath condition where different radio waves arrive from different

(a) Location I



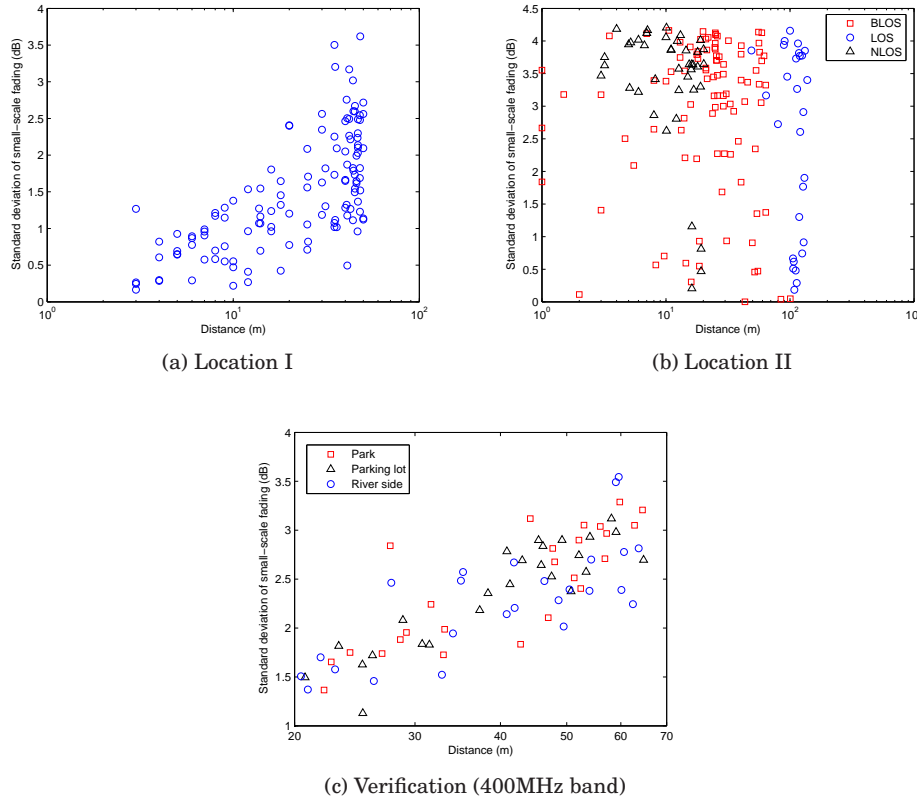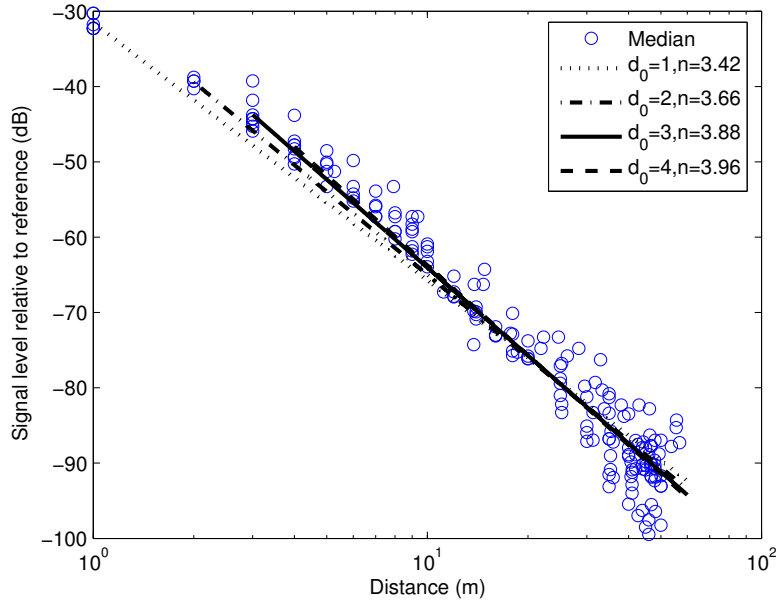(b) Location II



(c) Verification (400MHz band)

Fig. 24.   Standard deviation of measurement samples

directions with different time delays. When they combine vectorially at the receiver, the resultant signal can vary significantly over a small area. The reverse is true for LOS conditions where a significant number of signals transmitted far away still have a very strong single dominant path and thus a very low standard deviation for the small-scale fading in a small area.

## B. MODELLING THE RESULTS USING THE LOG-NORMAL PATH LOSS MODEL

In this appendix, we present results for the measured path loss exponent as well as the standard deviation for the log-normal path loss model as this is one of the most common path loss models in use. We first show the results obtained from the flat terrain in Section 4, then the results from the irregular terrain in Section 5.

Fig. 5 includes the best fit log-distance model (13) from the complete measurement results with $d_0 = 1$m as the reference. We see that it tends to slightly over estimate path loss at small distances and under estimate them at larger distances. Plotting the best fits using measurement results for $d_0 = 1, 2, 3, 4$m in Fig. 25, we can see that the slope of the fits converge somewhere between $d_0 = 3$ and $d_0 = 4$ for Location I, and that using a reference distance too close to the signal source may affect the accuracy of the model. However, this inflection point depends on the composition of the material of the propagation surface, and varies from location to location. Experimental results from [Martfnez-Sala et al. 2005] seem to confirm this, although they did not relate

Fig. 25.   Log-distance model with different $d_0$ at Location I

Table V. $n$ and $\sigma$ for different $d_0$ for Location I

| $d_0$ (m) | 1 | 2 | 3 | 4 |
|---|---|---|---|---|
| $n$ | 3.42 | 3.66 | 3.88 | 3.96 |
| $\sigma_{dB}$ | 5.07 | 4.69 | 4.74 | 4.83 |
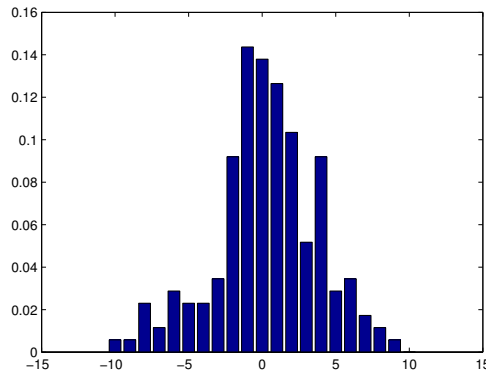


Fig. 26.   Probability distribution of signals' medians around predicted path loss ($d > 3$m)

the results to the surface's permittivity and conductivity. Table V shows the best fit $n$ values for different $d_0$s for the log-distance model.

In Fig. 26, we plot the histogram of the signal envelope medians after removing the log-distance ($d_0 = 3$m) trendlines for distances 3m and above from the reference source. We can see that the distribution tends to be log-normal with a $\sigma_{dB}$ of 3.48.

In the case of irregular terrain (Section 5), Fig. 27 shows the LSE log-distance fits for the different path types. As can be expected, the values of $n$ differ by quite a lot de-
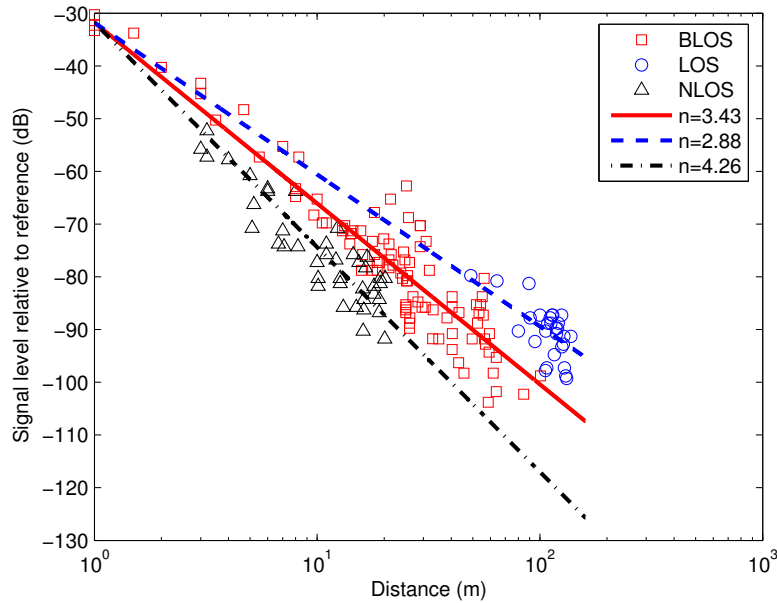
Fig. 27.   Log-distance best fit according to path type at Location II

Table VI. $n$ and $\sigma_{dB}$ for Location II

| Path Type | Total | BLOS | LOS | NLOS |
|-----------|-------|------|-----|------|
| $n$ | 3.35 | 3.43 | 2.88 | 4.26 |
| $\sigma_{dB}$ | 7.84 | 5.48 | 3.80 | 4.35 |

pending on the path type with LOS paths having the lowest rate of signal attenuation and NLOS paths having the highest. Using LSE, the fitted overall path loss exponent $n = 3.35$ with $\sigma_{dB} = 7.84$dB for all the sample points, calculated using $d_0 = 1$m ($d_0 = 3$m gives a similar result here due to LOS and NLOS paths causing a large deviation from the mean). We summarise the values of $n$ and $\sigma_{dB}$ for the log-distance fits for each path type in Table VI. While the log-normal shadowing model is useful when the terrain profile is unknown, a more accurate model can be obtained by taking into account the terrain profile.

## ACKNOWLEDGMENTS

## REFERENCES

ABDI, A., TEPEDELENLIOGLU, C., KAVEH, M., AND GIANNAKIS, G. 2001. On the estimation of the k parameter for the rice fading distribution. *IEEE Communications Letters 5,* 3, 92 –94.

ANDERSEN, J. B., RAPPAPORT, T. S., AND YOSHIDA, S. 1995. Propagation measurements and models for wireless communications channels. *IEEE Communications Magazine 33,* 1, 42 –49.

BUETTNER, M., YEE, G. V., ANDERSON, E., AND HAN, R. 2006. X-MAC: A Short Preamble MAC Protocol for Duty-Cycled Wireless Sensor Networks. In *Proceedings of the 4th International Conference on Embedded Networked Sensor Systems.* ACM, New York, NY, USA, 307–320.

BULLINGTON, K. 1947. Radio propagation at frequencies above 30 megacycles. *Proceedings of the IRE 35,* 10, 1122 – 1136.

CERPA, A., BUSEK, N., AND ESTRIN, D. 2003. SCALE: A tool for Simple Connectivity Assessment in Lossy Environments. Tech. rep., University of California, Los Angeles.

CERPA, A., WONG, J. L., POTKONJAK, M., AND ESTRIN, D. 2005. Temporal Properties of Low Power Wireless Links: Modeling and Implications on Multi-Hop Routing. In *MobiHoc '05: Proceedings of the 6th ACM international symposium on Mobile ad hoc networking and computing*. ACM, New York, NY, USA, 414–425.

CHONG, P. K., YOO, S., KIM, S. H., AND KIM, D. 2011. Wind-blown foliage and human induced fading in ground-surface narrowband communications at 400mhz. *IEEE Transactions on Vehicular Technology 60,* 4, 1326–1336.

COX, D. C., MURRAY, R. R., AND NORRIS, A. W. 1983. Measurements of 800mhz radio transmission into buildings with metallic walls. *The Bell System Technical Journal 9,* 62, 2695–2717.

DEEPAK, G., KRISHNAMACHARI, B., WOO, A., CULLER, D., ESTRIN, D., AND WICKER, S. 2002. Complex behavior at scale: An experimental study of low-power wireless sensor networks. Tech. Rep. Technical Report UCLA/CSD-TR 02-0013, UCLA.

EDWARDS, R. AND DURKIN, J. 1969. Computer prediction of service areas for v.h.f. mobile radio networks. *Proceedings of the Institution of Electrical Engineers 116,* 9, 1493 –1500.

EGLI, J. J. 1957. Radio propagation above 40 mc over irregular terrain. *Proceedings of the IRE 45,* 10, 1383 –1391.

FORAN, R. A., WELCH, T. B., AND WALKER, M. J. 1999. Very near ground radio frequency propagation measurements and analysis for military applications. In *IEEE Military Communications Conference Proceedings*. Vol. 1. 336 –340.

HASHIM, M. H. AND STAVROU, S. 2005. Wind influence on radio waves propagating through vegetation at 1.8 ghz. *IEEE Antenna and Wireless Propagation Letters 4*, 143 – 146.

HOFFMAN, H. AND COX, D. 1982. Attenuation of 900 mhz radio waves propagating into a metal building. *IEEE Transactions on Antennas and Propagation 30,* 4, 808 – 811.

IEEE. 1998. Ieee standard definitions of terms for radio wave propagation. *IEEE Std 211-1997*.

JOSHI, G. G., DIETRICH, C. B., ANDERSON, C. R., NEWHALL, W. G., DAVIS, W. A., ISAACS, J., AND BARNETT, G. 2005. Near-ground channel measurements over line-of-sight and forested paths. In *IEE Proceedings - Microwave, Antennas and Propagation*. 589 – 596.

KAJIWARA, A. 2000. Lmds radio channel obstructed by foliage. In *Proceedings IEEE International Conference on Communications*. Vol. 3. 1583–1587.

KARP, B. N. 2000. Geographic routing for wireless networks. Ph.D. thesis, Cambridge, MA, USA. AAI9988566.

KIM, H.-S. AND NARAYANAN, R. A. 2002. A new measurement technique for obtaining the complex relative permittivity of terrain surfaces. *IEEE Transactions on Geoscience and Remote Sensing 40,* 5, 1190 – 1194.

LEE, W. C. 1982. *Mobile Communications Engineering*. McGraw-Hill Professional.

LIU, S., FAN, K.-W., AND SINHA, P. 2009. Cmac: An energy-efficient mac layer protocol using convergent packet forwarding for wireless sensor networks. *ACM Transactions on Sensor Networks 5*, 29:1–29:34.

LONGLEY, A. G. AND RICE, P. L. 1968. Prediction of tropospheric radio transmission over irregular terrain, a computer method-1968. Tech. rep., U.S. Government Printing Office, Washington, DC. July. ESSA Tech. Rep. ERL 79-ITS 67.

MARTFNEZ-SALA, A., MOLINA-GARCIA-PARDO, J.-M., EGEA-LOPEZ, E., VALES-ALONSO, J., JUAN-LLACER, L., AND GARCIA-HARO, J. 2005. An accurate radio channel model for wireless sensor networks simulation. *Journal of Communications and Networks 7,* 4, 401–407.

NORTON, K. A. 1937. The physical reality of space and surface waves in the radiation field of radio antennas. *Proceedings of the IRE 25,* 9, 1192 – 1202.

NS2. 2009. *NS-2*. http://www.isi.edu/nsnam/ns/.

PARSONS, J. D. 1992. *The Mobile Radio Propagation Channel*. Wiley, New York, USA.

PERKINS, C., BELDING-ROYER, E., AND DAS, S. 2003. Ad hoc on-demand distance vector (aodv) routing.

QUALNET. 2009. *Qualnet*. http://www.scalable-networks.com/.

RAPPAPORT, T. S. 2001. *Wireless Communications: Principles and Practice*. Prentice Hall PTR, Upper Saddle River, NJ, USA.

SNR. SNR. http://www.snr.kr/.

SOHRABI, K., MANRIQUEZ, B., AND POTTIE, G. J. 1999. Near ground wideband channel measurement in 800-1000 mhz. In *Proceedings of the 49th IEEE Vehicular Technology Conference*. Vol. 1. 571 –574.

SOMMERFELD, A. 1909. Propagation of waves in wireless telegraphy. *Annals of Physics 28*, 665–737.

SU, W. AND ALZAGHAL, M. 2009. Channel propagation characteristics of wireless micaz sensor nodes. *Ad Hoc Networks 7,* 6, 1183 – 1193.

TEXAS INSTRUMENTS. 2008a. Cc1101 data sheet (rev. d). *http://focus.ti.com/*.

TEXAS INSTRUMENTS. 2008b. *Design Note DN505: RSSI Interpretation and Timing.* http://focus.ti.com/lit/an/swra114b/swra114b.pdf.

WAIT, J. R. 1998. The ancient and modern history of em ground-wave propagation. *IEEE Antennas and Propagation Magazine 40,* 5, 7 –24.

WELCH, T. B., WOOD, J. R., MCPARLIN, R. W., SCHULZE, L. K., FLAHERTY, T P., I., CARLONE HANSON, S. G., CAHILL, R. J., AND FORAN, R. A. 2000. Very near ground rf propagation measurements for wireless systems. In *IEEE Military Communications Conference Proceedings*. Vol. 3. 2556 –2558.

WONG, K. J. AND ARVIND, D. K. 2005. Specknets: new challenges for wireless communication protocols. *Third International Conference onInformation Technology and Applications, 2005. ICITA 2005. 2*, 728 – 733 vol.2.

WOO, A., TONG, T., AND CULLER, D. 2003. Taming the underlying challenges of reliable multihop routing in sensor networks. In *SenSys '03: Proceedings of the 1st international conference on Embedded networked sensor systems*. ACM, New York, NY, USA, 14–27.

WOYACH, K., PUCCINELLI, D., AND HAENGGI, M. 2006. Sensorless sensing in wireless networks: Implementation and measurements. In *Proc. 4th International Symposium on Modeling and Optimization in Mobile, Ad Hoc and Wireless Networks*. 1–8.

YOO, S., CHONG, P. K., AND KIM, D. 2009. S3: School zone safety system based on wireless sensor network. *Sensors 9,* 8, 5968–5988.

ZENNECK, J. 1907. Propagation of plane em waves along a plane conducting surface. *Annals of Physics 23*, 846–866.

ZHAO, J. AND GOVINDAN, R. 2003. Understanding Packet Delivery Performance in Dense Wireless Sensor Networks. In *SenSys '03: Proceedings of the 1st international conference on Embedded networked sensor systems*. ACM, New York, NY, USA, 1–13.

ZHOU, G., HE, T., KRISHNAMURTHY, S., AND STANKOVIC, J. A. 2004. Impact of Radio Irregularity on Wireless Sensor Networks. In *MobiSys '04: Proceedings of the 2nd international conference on Mobile systems, applications, and services*. ACM, New York, NY, USA, 125–138.

ZHOU, G., HE, T., KRISHNAMURTHY, S., AND STANKOVIC, J. A. 2006. Models and solutions for radio irregularity in wireless sensor networks. *ACM Transactions on Sensor Networks 2*, 221–262.

ZORZI, M. AND RAO, R. R. 2003. Geographic Random Forwarding (GeRaF) for Ad Hoc and Sensor Networks: Energy and Latency Performance. *IEEE Transactions on Mobile Computing 2,* 4, 349–365.